Acta Mech 224, 1741–1755 (2013)
DOI 10.1007/s00707-013-0831-4

Yingli Li · S. A. Meguid · Yiming Fu · Daolin Xu

Unified nonlinear quasistatic and dynamic analysis of RF-MEMS switches

Received: 6 September 2012 / Revised: 3 December 2012 / Published online: 22 March 2013

Abstract In this paper, the modified couple stress-based strain gradient theory is used to provide a unified nonlinear model of the quasistatic and dynamic behavior of an electrostatic microelectromechanical systems microbeam capacitive switch of the Euler–Bernoulli type. Our model not only accounts for the contact between the microbeam and the dielectric substrate using nonlinear springs and dampers, but also accounts for the system size by introducing an internal material length scale parameter. In view of the size of the microbeam and electrostatic gaps involved, Casimir and Van der Waals forces, damping force due to the squeeze membrane effect and electrostatic force with first-order fringing field effects were accounted for in our model. The resulting nonlinear system of PDEs was expanded into a coupled system using series expansion and integrated into ODEs using weighted residuals of the Galerkin type. To overcome the difficulties associated with the determination of the contact length, the Heaviside function for deflection was replaced with a Heaviside function for the contact length, and an iterative procedure was adopted to determine the contact length. To obtain the time variation of the microbeam, the dynamic system of equations was solved using Newmark's integration scheme. The outcome of our work shows the dependence of the pull-in voltage upon the inertia force, slenderness ratios of the microbeam, the electrostatic gap and the initial boundary conditions of the switch. In addition, we were also able to provide the full history of the microbeam past the pull-in threshold.

1 Introduction

Research on microelectromechanical systems (MEMS) has seen remarkable growth in the last three decades, stimulated both by their interesting physical properties and by their attractive applications potential. One of those appealing MEMS applications are radio frequency (RF) switches [1], which holds promise for replacing conventional solid-state switches for RF or microwave applications. RF-MEMS switches have lower insertion loss and higher isolation than solid-state switches, which are critical requirements for the next generation of communication systems. MEMS switches have the potential to replace PIN diodes, which are now widely used in current communication systems and can also be used in devices and systems for medical and military applications. For instance, the insertion loss of a RF-MEMS switch is only 0.05–0.2 dB at frequencies ranging from 1 to 100 GHz; this is in contrast to 0.3–1.2 dB for PIN diodes and 0.4–2.5 dB for FET switches in the same frequency regime. RF-MEMS have numerous benefits and applications that are extensively reviewed in [2]. RF-MEMS switches are now available in the market place. For RADAR applications, for instance, approximately 10,000 time-delay circuits are required, bringing the total number of RF switches to approximately

Y. Li · S. A. Meguid (✉)
Mechanics and Aerospace Design Laboratory, Department of Mechanical and Industrial Engineering,
University of Toronto, Toronto, ON M5S 3G8, Canada
E-mail: meguid@mie.utoronto.ca

Y. Li · Y. Fu · D. Xu
College of Mechanical and Vehicle Engineering, Hunan University, Changsha 410082, People's Republic of China

1/2 million [3]. Several hurdles remain unresolved and require the attention of the research community so as to ensure the reliability of RF-MEMS switches and turn them into commercially viable products. Indeed, long-term reliability is one of the major concerns in the use of RF-MEMS switches [4]. The failure modes of the microswitch have been identified to be either resistance increase with cycling leading to degraded performance or stiction which results in a fail-to-open malfunction. Another hurdle is the inability to obtain a sufficiently high switching speed at low actuation voltages with less bouncing. In fact, the true underlying mechanisms responsible for failures of the MEMS switches are not yet known or well understood because of the complexities involved in contact during their operation. In view of the fact that the structural dynamics of these microswitches can be a determining factor for the desired switching speed and pull-in contact history, their mechanical characterization is becoming an integral part of MEMS design and development.

A large body of work has been lately dedicated to the dynamic modeling of MEMS up to the pull-in; see, e.g., Refs. [5–7]. Gupta et al. [5] conducted experiments and simulations on the transient behavior of a microbeam driven by a dc voltage at varying ramp-rates. Nielson and Barbastathis [6], using a lumped-mass model of a parallel-plate actuator, found that pull-in occurs at half the electrostatic gap. The associated bifurcation was assumed to be the dynamic pull-in where the voltage was only 91.1 % of the static pull-in voltage. A similar conclusion was drawn by Fargas-Marquès and Shkel [8] based on a lumped-mass model, which was later verified experimentally in [9]. Elata and Bamberger [10] generated a stagnation curve that characterizes all those deflection states where an applied voltage can bring the microbeam to rest. Nayfeh et al. [7] generated frequency–response curves describing the resonant response of a clamped–clamped electrostatic microbeam. Modeling, analysis and experimental studies of the nonlinear dynamic behavior of MEMS devices have recently been reported in [11–14] and NEMS [15]. Most models concerning the dynamics of the microswitch concentrate only on certain aspects of the switch, such as the squeeze-film damping effect. For instance, Steeneken et al. [16] investigated the dynamics and squeeze-film damping of a capacitive RF-MEMS switch. Massad et al. [17] studied the dynamic behavior of a MEMS switch using the finite element method in which they coupled the switch dynamics with the electrostatic actuation. McCarthy et al. [18] presented a one-dimensional dynamic finite difference model, based on beam theory, which included squeeze-film damping and a linear contact spring to simulate the dynamics of an ohmic contact RF-MEMS switch both prior to and postcontact.

It has been experimentally observed that RF-MEMS switches oscillate a few times prior to making permanent contact with the fixed electrode [16–18]. This is due to the stored elastic energy in the microbeam. The existence of these bouncing increases the effective closing time of the switch. Meanwhile, the contact surface between the switch and the substrate may be damaged by a large impact force which can be much larger than the quasistatic contact force. This instantaneous high impact force may induce local hardening or pitting of contacting elements at the contact region. In addition, bouncing may result in material transfer or contact welding [19], which are not desirable for high-reliability switches. This behavior suggests that the dynamics of the switch is a significant factor in dictating the long-term performance of the switch. Decuzzi et al. [20,21] developed a model based on Euler–Bernoulli theory to study the bouncing dynamics of a resistive switch. They included van der Waals' force and a linear spring to represent the respective attractive and repulsive forces between the contact tip and the fixed electrode. Gee et al. [22] presented a dynamic model and examined the effect of the dynamics of the switch on its opening time. In that model, they used a fourth-order beam deflection equation and included the adhesion force due to both van der Waals' type forces and metal-to-metal bonds. Czaplewski et al. [23] used a dual pulse method to achieve a soft landing of the microswitch and presented the dynamic results of a RF-MEMS switch. However, they ignored the mechanical contact and squeeze-film damping effects.

Stiction failures are now posing another significant challenge to the commercial deployment of RF-MEMS switches. The prevalence of these failures has undermined the reliability of MEMS switches. In these failures, the switch structure deforms upon contact with the substrate in response to an actuation voltage beyond the pull-in threshold. When the actuation signal is removed, the switch fails to recover its initial equilibrium position. This is due to the surface forces between the switch and the substrate. Savkar and Murphy [24,25] and Savkar et al. [26] proposed a vibratory release mechanism to prevent microbeam stiction where an AC voltage, tuned to a resonance frequency of the microbeam, is applied to release the microbeam. Gorthi et al. [27] studied the pull-in behavior of cantilever microbeams past the pull-in threshold. Models of MEMS past pull-in are useful in analyzing MEMS impact actuators, such as that proposed by Bienstman et al. [28].

Liu et al. [29] found that when the initial gap is small, the Casimir and Van der Waals forces become comparable with the electrostatic force and may therefore significantly influence the dynamics of the microbeam. However, lacking an internal material length scale parameter, classical microbeam models presented

in the above-mentioned works cannot be used to interpret this micro-/nanostructure-dependent size effect. Therefore, it is necessary to extend these models using higher order (nonlocal) continuum theories [30] such as the one discussed in [31] to account for the length scale. Considering the difficulties in determining the structure-related length scale parameters [32,33], nonlocal models involving only one additional material length scale parameter, which can account for the approximate nature of beam theories and justify the paradoxes in nonlocal microbeam model [34], are desirable. A modified couple stress theory based on strain gradient has recently been proposed by Yang et al. [35], where the couple stress tensor is symmetric and only one internal material length scale parameter is introduced. Based on this new theory, new Euler–Bernoulli and Timoshenko beam models have been introduced by Park and Gao [36] and Ma et al. [37], respectively. Recently, some size-dependent phenomena in microstructure [38] and nanostructure [39,40] have successfully been explained using the above models. Noteworthy is the fact that research on modeling the behavior of MEMS past pull-in is relatively scarce.

In spite of the above excellent contributions, little work has been conducted to develop a comprehensive model to accurately predict the dynamic behavior of a microswitch. In this work, we develop such a comprehensive model which covers the important aspects pertaining to the quasistatic and dynamic behavior of a microswitch. In our current model, a modified couple stress theory based on strain gradients is employed to account for the size effect of the microbeam. The model also accounts for the nonlinear contact force of the microbeam. In addition, a mathematical model involving Van der Waals force, Casimir force and squeeze-film damping effect is developed to study the static and dynamic behavior of the RF-MEMS switch. In the numerical simulations, the microscopic size of the beam, its slenderness ratio, and the electrostatic gap on the static pull-in voltage and dynamic response of the switch are determined and discussed. Furthermore, the actuation parameters (actuation amplitude and time) for the operation of the switch are investigated.

2 Basic equations

Let us consider an electrostatically actuated fixed–fixed microbeam, with length L, width b and thickness h, as depicted in Fig. 1. A voltage drop $V(t)$ is applied across the beam and an overlapping electrode underneath it. A dielectric layer is fabricated on top of the electrode to avoid short circuit during oscillatory impact.

Assume $u_0(x,t)$ and $w(x,t)$are the displacements of the microbeam. According to the Euler–Bernoulli assumptions, the nonlinear strain-displacement relation for the microbeam can be expressed as

$$\begin{aligned} \varepsilon_x &= \varepsilon_0 + z\kappa(x,t) = u_{0,x}(x,t) + \frac{1}{2}w_{,x}(x,t)^2 - zw_{,xx}(x,t), \\ \chi_{xy} &= -w_{,xx}/2. \end{aligned} \tag{1}$$

And the constitutive relations are

$$\begin{aligned} \sigma_x &= E\varepsilon_x, \\ m_{xy} &= 2l^2\mu_0\chi_{xy} \end{aligned} \tag{2}$$

where E is Young's modulus, $\mu_0 = E/2(1+\nu)$ is Lame's coefficient, and l is a material length scale parameter.

According to Hamilton's principle, we have

$$\delta \int_{t_1}^{t_2} (T + W - U)\mathrm{d}t = 0 \tag{3}$$

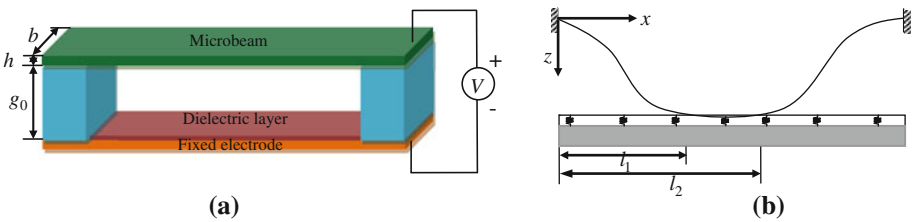

Fig. 1 Model of RF-MEMS capacitive switch. **a** Fixed–fixed MEMS beam; **b** sketch of the RF-MEMS switch past pull-in

where T is the kinetic energy, W is the work done by the external force, and U is the strain energy. Based on the modified couple stress theory [35], the variation of the strain energy can be written as

$$\begin{aligned}\delta U &= \int_{\Omega} \left(\sigma_{ij}\delta\varepsilon_{ij} + m_{ij}\delta\chi_{ij}\right) \mathrm{d}v = \int_{\Omega} \left(\sigma_x\delta\varepsilon_x + 2m_{xy}\delta\chi_{xy}\right) \mathrm{d}v \\ &= \int_{\Omega} \left[\sigma_x\delta\left(u_{0,x} + \frac{1}{2}w_{,x}^2 - zw_{,xx}\right) + 2m_{xy}\delta\left(-\frac{1}{2}w_{,xx}\right)\right] \mathrm{d}v \\ &= \int_0^L \left[-N_{,x}\delta u_0 - (Nw_{,x})_{,x}\delta w + M_{,xx}\delta w + Y_{,xx}\delta w\right] \mathrm{d}x \end{aligned} \tag{4}$$

where the stress resultants are

$$\begin{aligned} N &= b\int_{-h/2}^{h/2} \sigma_x \mathrm{d}z = b\int_{-h/2}^{h/2} E\left(u_{0,x} + \frac{1}{2}w_{,x}^2 - zw_{,xx}\right) \mathrm{d}z = EA\left(u_{0,x} + \frac{1}{2}w_{,x}^2\right), \\ M &= -b\int_{-h/2}^{h/2} z\sigma_x \mathrm{d}z = -b\int_{-h/2}^{h/2} zE\left(u_{0,x} + \frac{1}{2}w_{,x}^2 - zw_{,xx}\right) \mathrm{d}z = EIw_{,xx}, \\ Y &= -b\int_{-h/2}^{h/2} m_{xy} \mathrm{d}z = -b\int_{-h/2}^{h/2} 2l^2\mu_0\left(-\frac{1}{2}w_{,xx}\right) \mathrm{d}z = Al^2\mu_0 w_{,xx}. \end{aligned}$$

And $I = bh^3/12$, $A = bh$ are the respective second moments of area and area of the microbeam.

Similarly, the variation of work done by the external forces is

$$\delta W = \int_0^L q\delta w dx \tag{5}$$

where the force

$$q = F_e - F_v + F_{va} + F_c - F_{\mathrm{con}} \tag{6}$$

and where F_e is the electrostatic force and is given by [41]

$$F_e = \frac{1}{2}\frac{\varepsilon_v b V^2}{(g_0 - w)^2}\left(1 + 0.65\frac{(g_0 - w)}{b}\right) \tag{7}$$

with the first-order fringing field effect included. The absolute dielectric constant in vacuum is taken to be $\varepsilon_v = 8.8542 \times 10^{-12}$F/m. F_v is the damping force caused by the squeezing membrane effect. In accordance with Reynolds' equation, it can be written as [42]

$$F_v = \frac{\nu_0 b^3}{(g_0 - w)^3}\frac{\partial w}{\partial t} \tag{8}$$

where ν_0 is the viscosity coefficient of air $\nu_0 = 17.9 \times 10^{-6}$. The Van der Waals force F_{va} according to [29] is assumed to take the form

$$F_{va} = \frac{A_{12} b}{6\pi(g_0 - w)^3} \tag{9}$$

where the Hamaker constant $A_{12} = 4 \times 10^{-20}$J. The Casimir force according to [29] is

$$F_c = \frac{\pi^2 \hbar c b}{240(g_0 - w)^4} \tag{10}$$

where the Planck constant $\hbar = 6.625 \times 10^{-34}$J s, and the speed of light $c = 3 \times 10^8$m/s. F_{con} is the contact force. Using a nonlinear spring model to represent contact, we obtain [43]

$$F_{\text{con}} = k_{\text{con}}(w - g_0)^n(1 + \mu w_{,t})H(w - g_0). \tag{11}$$

If we neglect the contact nonlinearities, then $n = 1$ in the above expression. In Eq. (11), the Heaviside function $H(w - g_0)$ ensures that the contact force is applied only at those locations where $w \geq g_0$, viz.,

$$H(w - g_0) = \begin{cases} 0, & w < g_0 \\ 1, & w \geq g_0. \end{cases} \tag{12}$$

Furthermore, the variation of kinetic energy can be expressed as

$$\int_{t_1}^{t_2} \delta T \, \mathrm{d}t = \int_{t_1}^{t_2} \left(-\rho A \int_0^L w_{,tt} \delta w \mathrm{d}x \right) \mathrm{d}t. \tag{13}$$

Substituting Eqs. (4)–(13) into Eq. (3), we obtain the following equilibrium equation for the microbeam:

$$\begin{aligned} &\left(EI + \mu_0 A l^2\right) \frac{\partial^4 w}{\partial x^4} + \rho A \frac{\partial^2 w}{\partial t^2} + \frac{\nu_0 b^3}{(g_0 - w)^3} \frac{\partial w}{\partial t} = \left[P_r + \frac{EA}{2L} \int_0^L \left(\frac{\partial w}{\partial x} \right)^2 \mathrm{d}x \right] \frac{\partial^2 w}{\partial x^2} + \frac{1}{2} \frac{\varepsilon_v b V^2}{(g_0 - w)^2} \\ &\times \left[1 + 0.65 \frac{(g_0 - w)}{b} \right] + \frac{A_{12} b}{6\pi (g_0 - w)^3} + \frac{\pi^2 \hbar c b}{240 (g_0 - w)^4} - k_{\text{con}}(w - g_0)^n \left(1 + \mu \frac{\partial w}{\partial t} \right) H(w - g_0) \end{aligned} \tag{14}$$

where P_r is the initial residual axial load caused by thermal mismatch and/or manufacturing. Introducing the following dimensionless parameters:

$$\begin{aligned} &\xi = \frac{x}{L}, \ W = \frac{w}{g_0}, \ \tau = \frac{t}{T}, \ \gamma = \frac{l}{h}, \ \alpha_1 = \frac{L^4 \nu_0 b^3}{(EI + \mu_0 A l^2) g_0^3 T}, \ \alpha_2 = \frac{EA g_0^2}{2(EI + \mu_0 A l^2)}, \ \bar{P} = \frac{P_r L^2}{(EI + \mu_0 A l^2)}, \\ &\alpha_3 = \frac{L^4 \varepsilon_v b V_0^2}{2(EI + \mu_0 A l^2) g_0^3}, \ T = \sqrt{\frac{L^4 \rho A}{(EI + \mu_0 A l^2)}}, \ \alpha_4 = \frac{L^4 k_{\text{con}} g_0^{n-1}}{(EI + \mu_0 A l^2)}, \ \alpha_5 = \frac{L^4 A_{12} b}{6\pi (EI + \mu_0 A l^2) g_0^4}, \\ &\alpha_6 = \frac{L^4 \pi^2 \hbar c b}{240 (EI + \mu_0 A l^2) g_0^5}, \ \beta_1 = 0.65 \frac{g_0}{b}, \ \beta_2 = \frac{\mu g_0}{T}, \ \bar{V} = \frac{V}{V_0} \end{aligned} \tag{15}$$

where V_0 is a unit voltage, the equilibrium equation (14) of the microbeam can be rewritten as

$$\begin{aligned} &\frac{\partial^4 W}{\partial \xi^4} + \frac{\partial^2 W}{\partial \tau^2} + \alpha_1 \frac{1}{(1 - W)^3} \frac{\partial W}{\partial \tau} = \left[\bar{P} + \alpha_2 \int_0^1 \left(\frac{\partial W}{\partial \xi} \right)^2 \mathrm{d}\xi \right] \frac{\partial^2 W}{\partial \xi^2} + \frac{\alpha_3 \bar{V}^2}{(1 - W)^2} \left[1 + \beta_1 (1 - W) \right] \\ &- \alpha_4 (W - 1)^n \left(1 + \beta_2 \frac{\partial W}{\partial \tau} \right) H(W - 1) + \frac{\alpha_5}{(1 - W)^3} + \frac{\alpha_6}{(1 - W)^4}. \end{aligned} \tag{16}$$

Expanding the terms whose denominator has $(1 - W)$ in the above equation into a third-order Taylor series, we get

$$\begin{aligned} &\frac{\partial^4 W}{\partial \xi^4} + \frac{\partial^2 W}{\partial \tau^2} + \alpha_1 (1 + 3W + 6W^2) \frac{\partial W}{\partial \tau} = \left[\bar{P} + \alpha_2 \int_0^1 \left(\frac{\partial W}{\partial \xi} \right)^2 \mathrm{d}\xi \right] \frac{\partial^2 W}{\partial \xi^2} + \left[(1 + \beta_1) + (2 + \beta_1) W \right. \\ &\left. + (3 + \beta_1) W^2 + (4 + \beta_1) W^3 \right] \alpha_3 \bar{V}^2 - \alpha_4 (W - 1)^n \left(1 + \beta_2 \frac{\partial W}{\partial \tau} \right) H(W - 1) \\ &+ \alpha_5 \left(1 + 3W + 6W^2 + 10W^3 \right) + \alpha_6 \left(1 + 4W + 10W^2 + 20W^3 \right). \end{aligned} \tag{17}$$

The ratios of the coefficients of the electrostatic force $\alpha_3\bar{V}^2$, Van der Waals force α_5 and Casimir force α_6 are $\varepsilon_v V^2 : A_{12}/(3\pi g_0) : \pi^2\hbar c/(120 g_0^2)$, that is, $8.8542\times10^{-12}V^2$: $4.24413\times10^{-21}/g_0$: $1.63465\times10^{-26}/g_0^2$. It means that only when the gap g_0 is of the order of nanometers (10^{-9} m), the Van der Waals force and Casimir force will be of comparable magnitude to the electrostatic force. For example, when the microbeam is pulled in toward the dielectric layer, the gap between the switch and substrate is reduced, and as a result the Van der Waals force and Casimir force between these two components will play a role in the effective response of the switch.

Let us now select a dimensionless boundary condition, such that

$$\xi = 0, 1 : W = \frac{\partial W}{\partial \xi} = 0. \tag{18}$$

We use the Galerkin method to convert Eq. (17) into a system of nonlinear ordinary differential equations. Therefore, we assume that the solution of Eq. (17) is of the following form:

$$W(\xi,\tau) = \sum_{j=1}^{N} \phi_j(\xi)\eta_j(\tau) \tag{19}$$

where $\eta_j(\tau)$ is a function of time and $\phi_j(\xi)$ is the basis function of the Galerkin reduction. To ensure both accuracy and efficiency, we carried out a number of tests and concluded that $N = 5$ is sufficient. Since both the structure and the load are symmetrical, only symmetric shape functions are envisaged. Furthermore, we use the undamped mode shapes of a fixed–fixed microbeam without axial extension as the basis function such that

$$\phi_j(\xi) = \cosh(\beta_j\xi) - \cos(\beta_j\xi) - \frac{\cosh(\beta_j) - \cos(\beta_j)}{\sinh(\beta_j) - \sin(\beta_j)}\left[\sinh(\beta_j\xi) - \sin(\beta_j\xi)\right]. \tag{20}$$

The values of β_j are obtained by solving the following characteristic equation:

$$\cosh(\beta_j)\cos(\beta_j) = 1. \tag{21}$$

To simplify Galerkin's integration scheme, the Heaviside function $H(W-1)$ is replaced by $H(\xi - l_1) - H(\xi - l_2)$, where l_1 and l_2 represent the ends of the contact length, as shown in Fig. 1b. In the case when there is no contact, $l_1 = l_2 = 0.5$.

After substituting Eq. (19) into Eq. (17), we multiply the resulting equation by $\phi_k(\xi)$ and integrate over the domain. Making use of the orthogonality of the mode shapes ($\int_0^1 \phi_j\phi_k \mathrm{d}\xi = \delta_{jk}$), the following nonlinear ordinary differential equations with the time-dependent function $\eta_k(\tau)(k = 1, 2, \ldots, 5)$ are obtained:

$$\begin{aligned}
&\ddot{\eta}_k + \alpha_1\dot{\eta}_k + 3\alpha_1\sum_{i,j=1}^{N}\eta_i\dot{\eta}_j\int_0^1\phi_i\phi_j\phi_k\mathrm{d}\xi + 6\alpha_1\sum_{i,j=1}^{N}\eta_i^2\dot{\eta}_j\int_0^1\phi_i^2\phi_j\phi_k\mathrm{d}\xi + \sum_{j=1}^{N}\eta_j\int_0^1\phi''''_j\phi_k\mathrm{d}\xi - \bar{P}\sum_{j=1}^{N}\eta_j\int_0^1\phi''_j\phi_k\mathrm{d}\xi \\
&= \alpha_2\sum_{j,l,m=1}^{N}\eta_j\eta_l\eta_m\int_0^1\phi'_l\phi'_m\mathrm{d}\xi\int_0^1\phi''_j\phi_k\mathrm{d}\xi + \alpha_3\bar{V}^2\left[(1+\beta_1)\int_0^1\phi_k\mathrm{d}\xi + (2+\beta_1)\eta_k + (3+\beta_1)\sum_{j=1}^{N}\eta_j^2\int_0^1\phi_j^2\phi_k\mathrm{d}\xi\right. \\
&\quad \left.+(4+\beta_1)\sum_{j=1}^{N}\eta_j^3\int_0^1\phi_j^3\phi_k\mathrm{d}\xi\right] - \bar{F}_{\mathrm{con}} + (\alpha_5+\alpha_6)\int_0^1\phi_k\mathrm{d}\xi + (3\alpha_5+4\alpha_6)\eta_k + (6\alpha_5+10\alpha_6)\sum_{j=1}^{N}\eta_j^2\int_0^1\phi_j^2\phi_k\mathrm{d}\xi \\
&\quad +(10\alpha_5+20\alpha_6)\sum_{j=1}^{N}\eta_j^3\int_0^1\phi_j^3\phi_k\mathrm{d}\xi
\end{aligned} \tag{22}$$

with the dimensionless contact force given by

$$\bar{F}_{\mathrm{con}} = \begin{cases}
\alpha_4\int_0^1\phi_k\left[H(\xi-l_1)-H(\xi-l_2)\right]\mathrm{d}\xi - 3\alpha_4\sum_{j=1}^{N}\eta_j\int_0^1\phi_j\phi_k\left[H(\xi-l_1)-H(\xi-l_2)\right]\mathrm{d}\xi \\
+3\alpha_4\sum_{j=1}^{N}\eta_j^2\int_0^1\phi_j^2\phi_k\left[H(\xi-l_1)-H(\xi-l_2)\right]\mathrm{d}\xi - \alpha_4\sum_{j=1}^{N}\eta_j^3\int_0^1\phi_j^3\phi_k\left[H(\xi-l_1)-H(\xi-l_2)\right]\mathrm{d}\xi \\
+\alpha_4\beta_2\sum_{j=1}^{N}\dot{\eta}_j\int_0^1\phi_j\phi_k\left[H(\xi-l_1)-H(\xi-l_2)\right]d\xi - 3\alpha_4\beta_2\sum_{i,j=1}^{N}\eta_i\dot{\eta}_j\int_0^1\phi_i\phi_j\phi_k\left[H(\xi-l_1)-H(\xi-l_2)\right]\mathrm{d}\xi \\
+3\alpha_4\beta_2\sum_{i,j=1}^{N}\eta_i^2\dot{\eta}_j\int_0^1\phi_i^2\phi_j\phi_k\left[H(\xi-l_1)-H(\xi-l_2)\right]\mathrm{d}\xi - \alpha_4\beta_2\sum_{i,j=1}^{N}\eta_i^3\dot{\eta}_j\int_0^1\phi_i^3\phi_j\phi_k\left[H(\xi-l_1)-H(\xi-l_2)\right]\mathrm{d}\xi\,(n=3) \\
\alpha_4\int_0^1\phi_k\left[H(\xi-l_1)-H(\xi-l_2)\right]\mathrm{d}\xi - \alpha_4\sum_{j=1}^{N}\eta_j\int_0^1\phi_j\phi_k\left[H(\xi-l_1)-H(\xi-l_2)\right]\mathrm{d}\xi \\
+\alpha_4\beta_2\sum_{j=1}^{N}\dot{\eta}_j\int_0^1\phi_j\phi_k\left[H(\xi-l_1)-H(\xi-l_2)\right]\mathrm{d}\xi - \alpha_4\beta_2\sum_{i,j=1}^{N}\eta_i\dot{\eta}_j\int_0^1\phi_i\phi_j\phi_k\left[H(\xi-l_1)-H(\xi-l_2)\right]\mathrm{d}\xi\,(n=1).
\end{cases} \tag{23}$$

Noting that the first mode should be the dominant mode of the system, the modal expansion presented in Eq. (19) can be approximated by a single term, when only the $j = 1$ term in Eq. (19) is considered and letting $n = 1, \phi_1(\xi) = \phi(\xi), \eta_1(\tau) = \eta(\tau)$. Consequently, Eq. (22) becomes

$$\begin{aligned}\ddot{\eta} + \alpha_1\left(a_2 + 3a_3\eta + 6a_4\eta^2\right)\dot{\eta} + \omega^2\eta = \alpha_2 a_6 a_7\eta^3 + [(1+\beta)a_1 + (3+\beta)a_3\eta^2 \\ +(4+\beta)a_4\eta^3]\alpha_3\bar{V}^2 - \alpha_4\left[a_1' - a_2'\eta + \beta_2\left(a_2' - a_3'\eta\right)\dot{\eta}\right] + (\alpha_5+\alpha_6)\,a_1 + (3\alpha_5+4\alpha_6)\,a_2\eta \\ + (6\alpha_5+10\alpha_6)\,a_3\eta^2 + (10\alpha_5+20\alpha_6)\,a_4\eta^3 \end{aligned} \tag{24}$$

where $\omega^2 = a_0 - \bar{P}a_6 - \alpha_3(2+\beta_1)a_2\bar{V}^2$ is the natural frequency of the microbeam in the absence of damping, and

$$a_0 = \int_0^1 \phi\phi'''\mathrm{d}\xi,\ a_i = \int_0^1 \phi^i\mathrm{d}\xi,\ a_i' = \int_0^1 \phi^i\left(H\left(\xi - l_1\right) - H\left(\xi - l_2\right)\right)\mathrm{d}\xi (i = 1, 2, 3),$$

$$a_6 = \int_0^1 \phi''\phi\mathrm{d}\xi,\ a_7 = \int_0^1 (\phi')^2\mathrm{d}\xi$$

where $a_2 = 1$, " $'$ " represents the derivatives with respect to coordinate ξ and "$\cdot$" denotes the derivatives with respect to the normalized time τ. Introducing the variables $x_1 = \eta, x_2 = \dot{\eta}$, Eq. (24) can be rewritten in the following first-order derivative form:

$$\begin{aligned}\dot{x}_1 &= x_2, \\ \dot{x}_2 &= -\alpha_1\left(a_2 + 3a_3x_1 + 6a_4x_1^2\right)x_2 - \omega^2x_1 + \alpha_2a_6a_7x_1^3 + \left[(1+\beta)a_1 + (3+\beta)a_3x_1^2 + (4+\beta)a_4x_1^3\right]\alpha_3\bar{V}^2 \\ &\quad -\alpha_4\left[(a_1' - a_2'x_1) + \beta_2\left(a_2' - a_3'x_1\right)x_2\right] + (\alpha_5+\alpha_6)\,a_1 + (3\alpha_5+4\alpha_6)\,a_2x_1 \\ &\quad + (6\alpha_5+10\alpha_6)\,a_3x_1^2 + (10\alpha_5+20\alpha_6)\,a_4x_1^3. \end{aligned} \tag{25}$$

When the microbeam is simplified to a mass-spring system, its dynamic equation is in a similar form to that of Eq. (25). The contact lengths l_1 and l_2 are determined iteratively at every load step by integrating the differential equations provided in Eqs. (22) or (25) using Newmark's integration scheme.

3 Numerical results and discussions

To demonstrate the validity and robustness of our model, let us select the following geometric parameters: $L = 210\ \mu\mathrm{m}$, $b = 100\ \mu\mathrm{m}$, $h = 1.5\ \mu\mathrm{m}$ and $g_0 = 1.18\ \mu\mathrm{m}$, and the following material parameters: $E = 166\ \mathrm{GPa}$, $\nu = 0.3$, $\rho = 2332\ \mathrm{kg/m^3}$, $k_{\mathrm{con}}^{(1)} = 4.7 \times 10^{11}$, $k_{\mathrm{con}}^{(3)} = 4.7 \times 10^{25}$ and $\mu = 0.8$ for the microbeam. The initial residual axial load is assumed to be $P_r = 0.9 \times 10^{-3}$ N, and the initial condition is assumed to be $\eta_k(0) = 0, \dot{\eta}_k(0) = 0$.

3.1 Static analysis of the microbeam

First, we consider the microbeam under DC voltage. By ignoring the inertia and damping forces, Eq. (17) can be degenerated to

$$\begin{aligned}\frac{\partial^4 W}{\partial\xi^4} = \left[\bar{P} + \alpha_2\int_0^1\left(\frac{\partial W}{\partial\xi}\right)^2\mathrm{d}\xi\right]\frac{\partial^2 W}{\partial\xi^2} + \left[(1+\beta_1) + (2+\beta_1)W\right. \\ \left.+(3+\beta_1)W^2 + (4+\beta_1)W^3\right]\alpha_3\bar{V}^2 - \alpha_4(W-1)^{n-1}H(W-1) \\ +\alpha_5\left(1 + 3W + 6W^2 + 10W^3\right) + \alpha_6\left(1 + 4W + 10W^2 + 20W^3\right). \end{aligned} \tag{26}$$

After Galerkin's first-order truncation, the above equation reduces to

$$(a_0 - \bar{P}a_6)\eta = \alpha_2 a_6 a_7 \eta^3 + \alpha_3 \bar{V}^2 \left[(1+\beta_1)a_1 + (2+\beta_1)a_2\eta + (3+\beta_1)\,a_3\eta^2 + (4+\beta_1)a_4\eta^3\right] - \alpha_4 \left(a_1 - 3a_2\eta + 3a_3\eta^2 - a_4\eta^3\right) H(\phi\eta - 1) + \alpha_5 \left(a_1 + 3a_2\eta + 6a_3\eta^2 + 10a_4\eta^3\right) + \alpha_6 \left(a_1 + 4a_2\eta + 10a_3\eta^2 + 20a_4\eta^3\right). \tag{27}$$

In order to evaluate the accuracy of our model, we made a number of validation tests with earlier work by other researchers. Let us consider the case prior to the pull-in. In this case, the contact force will not play a role. Earlier work presented in reference [43] did not account for Van der Waals force, Casimir force and the modified couple stress theory. Accordingly, Eq. (27) reduces to

$$\bar{V}(\eta) = \sqrt{\frac{(a_0 - \bar{P}a_6)\eta - \alpha_2 a_6 a_7 \eta^3}{\left[(1+\beta_1)a_1 + (2+\beta_1)a_2\eta + (3+\beta_1)a_3\eta^2 + (4+\beta_1)a_4\eta^3\right]\alpha_3}}. \tag{28}$$

Hence, the pull-in voltage of the switch can be obtained by ensuring the instability condition $\mathrm{d}\bar{V}/\mathrm{d}\eta = 0$, i.e.,

$$\frac{\mathrm{d}}{\mathrm{d}\eta}\sqrt{\frac{(a_0 - \bar{P}a_6)\eta - \alpha_2 a_6 a_7 \eta^3}{\left[(1+\beta_1)a_1 + (2+\beta_1)a_2\eta + (3+\beta_1)a_3\eta^2 + (4+\beta_1)a_4\eta^3\right]\alpha_3}} = 0. \tag{29}$$

We obtain η_{pi} by solving Eq. (29), and substitute it into Eq. (28) to obtain the pull-in voltage $\bar{V}(\eta_{pi})$. This leads us to determine the normalized displacement amplitude $\eta_{pi} = 0.391899$. This value corresponds to a normalized deflection $W = 0.622393$ and a corresponding pull-in voltage $\bar{V}(\eta_{pi}) = 29.9873$, which agrees well with the result of [43].

For the 1D effective MEMS model presented by [44], the pull-in voltage $V_{pi} = \sqrt{\frac{8K_{\mathrm{eff}}g_0^3}{27\varepsilon A}}$ and deflection $w = g_0/3$ is determined from $V = \frac{2K_{\mathrm{eff}}}{\varepsilon A}\left(g_0^2 w - 2g_0 w^2 + w^3\right)$. However, the midpoint deflection $W = 0.622393$ obtained from our model is larger than 1/3. This is because the initial residual tensile load and geometric nonlinearity are considered in our model. The nonlinear terms lead to an increase in the stiffness of the switch. Meanwhile, the electrostatic force is approximated by Taylor series, which is less than the actual actuating load. In fact, we further simplify our model by ignoring the geometric nonlinearity, the residual stresses and the fringe field effects of the electrostatic force by setting $\bar{P} = \alpha_2 = \beta_1 = 0$, and Eq. (27) reduces to

$$a_0\eta = \alpha_3 \bar{V}^2 \left(a_1 + 2a_2\eta + 3a_3\eta^2 + 4a_4\eta^3\right). \tag{30}$$

Accordingly, the pull-in voltage can be determined by

$$\bar{V}(\eta) = \sqrt{\frac{a_0\eta}{\alpha_3\left(a_1 + 2a_2\eta + 3a_3\eta^2 + 4a_4\eta^3\right)}},\quad \frac{\mathrm{d}}{\mathrm{d}\eta}\sqrt{\frac{a_0\eta}{\alpha_3\left(a_1 + 2a_2\eta + 3a_3\eta^2 + 4a_4\eta^3\right)}} = 0. \tag{31}$$

From Eq. (31), one can obtain $\eta_{pi} = 0.310923$ ($W_{pi} = 0.493792$) and pull-in voltage $\bar{V}(\eta_{pi}) = 25.9389$. The influence of the geometric nonlinearity, the residual stresses and the fringe field effects of the electrostatic force on the stiffness of the microbeam is reflected in the reduction in the pull-in voltage from almost 30 to 26, which represents 13.5 % reduction. It is clear from our work that the assumption of the one-dimensional mass-spring model adopted in reference [44] underestimates the pull-in actuating voltage and the corresponding deflection.

In all the following figures, the coordinate label W_0 denotes the normalized displacement of the midpoint of the microbeam and $\bar{V}$ denotes the normalized applied voltage. Figure 2 shows the variation of the deflection of the microbeam with the increase in the actuating voltage. It can be observed from the figure that when the deflection of microbeam center $W_{pi} = 0.622393$, the microbeam loses its stability and is pulled in. This effectively means that the pull-in voltage of the switch is $\bar{V}_{pi} = 29.9873$. This agrees with the findings of [43,45,46]. We further conducted a high-resolution three-dimensional finite element analysis using the commercial code ANSYS under the same stipulated conditions. The microbeam is discretised into 3D 20-node structural solid elements (Solid186), and the gap was modeled using 3D 20-node couple-field solid elements (Solid226). The insert in Fig. 2 shows the discretised geometry of the microbeam and the electrostatic gap. The FE results are superimposed on our analytical model prediction, denoted by the square symbols on that figure, and they reveal excellent agreement.

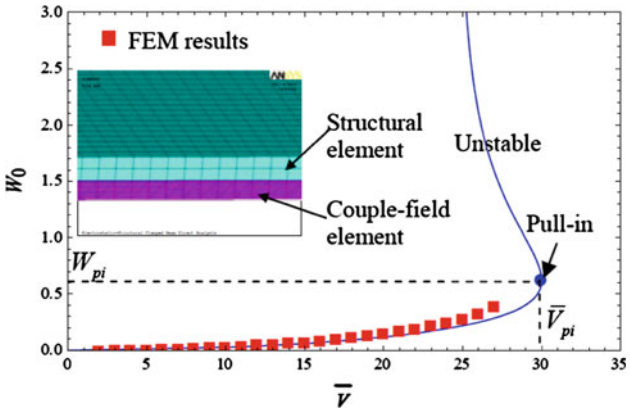

Fig. 2 Variation of microbeam normalized deflection against applied normalized voltage

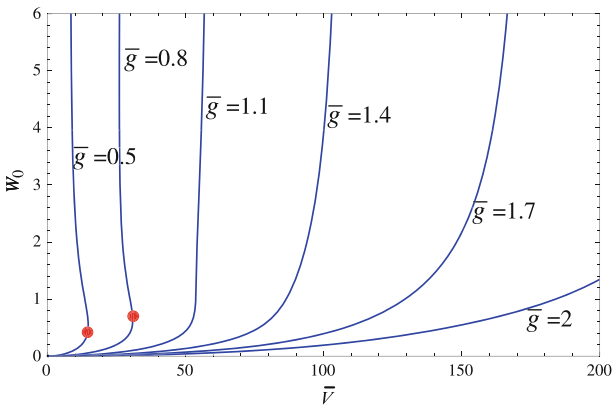

Fig. 3 Effect of normalized gap g_0/h on the normalized voltage–deflection V–W relationship

Figure 3 shows the change in the microbeam midpoint normalized deflection with the normalized actuation voltage for different values of normalized electrostatic gap $\bar{g} = g_0/h$. It can be observed that larger gaps lead to slower midpoint deflection with the increase in normalized actuation voltage. This indicates the need for larger pull-in voltage to compensate for the increase in the gap and the extended travel.

In all the previous validation tests, we used Galerkin first-order truncation. In the following, we will use Galerkin fifth-order truncation [$N = 5$ in Eq. (19)]. This will allow us to more accurately study the effect of the pertinent parameters upon the pull-in voltage and the resulting microbeam deflection as well as the associated contact using Eq. (22), where $\eta_k (k = 1, 2, \ldots, 5)$ is independent of time.

Figure 4 shows the midpoint of the microbeam deflection with the increase in the DC voltage. The figure shows that the normalized deflection of the microbeam increases with the increase in the actuating voltage. The rate of increase accelerates until the pull-in occurs at $\bar{V} = 30$, which agrees well with the pull-in voltage obtained from Eq. (29). The slight difference between these two values is due to the different orders of basis functions used. Specifically, in Eq. (29), only the first-order shape function is included in the calculation, and in Fig. 4 the first five orders are used in the calculation. The relation between the actuation voltage and the midpoint deflection of the microbeam in the present study agrees well with the findings of [43]. The microbeam is pulled in and remains in contact with the substrate as the voltage increases beyond that pull-in voltage. In this analysis, the contact stiffness k_{con} is chosen sufficiently high such that the maximum penetration of the microbeam into the substrate is kept to a minimum ($< 1\,\%$ of the microbeam thickness). From Fig. 4, it can be observed that the linear and nonlinear contact forces provide comparable results with minor deviation ($0.013\,\%$). In view of this, we used linear contact ($n = 1$) throughout the remainder of the study.

Figure 5 shows the variation of the normalized pull-in voltage and the material length scale parameter. It can be observed that the increase in the characteristic length parameter results in a dramatic increase in the pull-in voltage of the MEMS switch. Therefore, the modified couple stress theory should be employed in

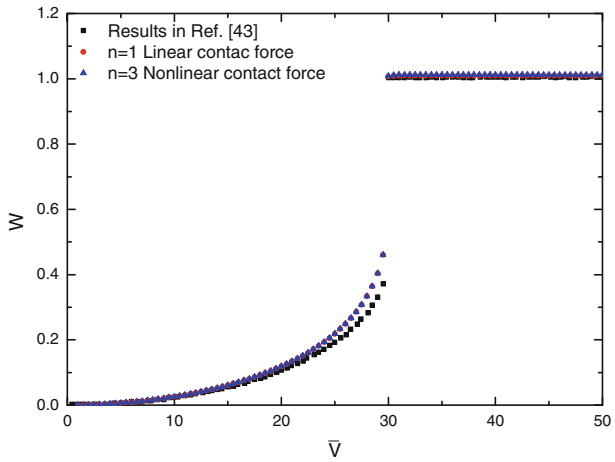

Fig. 4 Midpoint microbeam normalized deflection versus normalized actuating DC voltage

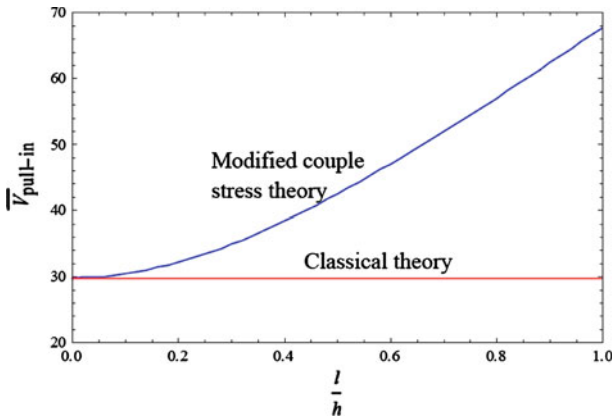

Fig. 5 Effect of characteristic length parameter on normalized pull-in voltage of the RF-MEMS switch

the design of MEMS devices in order to avoid underestimating the pull-in voltage of the device that could ultimately lead to switch pull-in failure.

Examining Figs. 6 and 3 jointly, it can be seen that the normalized actuating voltage increases nonlinearly with an increase in the normalized gap $\bar{g}$ for the two types of end supports considered in this study. It can be seen that for the same normalized gap the cantilever microbeam requires much lower pull-in voltage as opposed to the fixed–fixed support. For example, for a normalized gap of 0.8, the cantilever microbeam requires normalized pull-in voltage of 5, whereas the fixed–fixed microbeam requires 30; that is 6 times.

Figure 7 depicts the effect of microbeam geometry and initial residual axial load upon the normalized pull-in voltage. It can be observed from the figure that the increase in the slenderness of the microbeam $\bar{L}$ (L/h) leads to a reduction in the pull-in voltage. This is expected because of its direct relationship to the stiffness of the microbeam. The three curves in Fig. 7 represent the variation of the pull-in voltage with the initial residual axial load. Comparing the three curves, it can be observed that the presence of a compressive residual load leads to a reduction in the pull-in voltage as opposed to the stress-free beam or a beam containing tensile residual axial load. This is because the resistance to the pull-in bending loads introduced by the compressive axial load as opposed to the effect of tensile residual loads.

3.2 Dynamic analysis of the microbeam

In this section, we study the dynamic behavior of the microswitch by including the effects of the inertia forces and damping force [as shown in Eq. (22)]. If we neglect damping, $\alpha_1 = 0, \beta_2 = 0$, then the normalized dynamic pull-in voltage is reduced to 28.58 as depicted in Fig. 8a. This is due to the kinetic energy of the

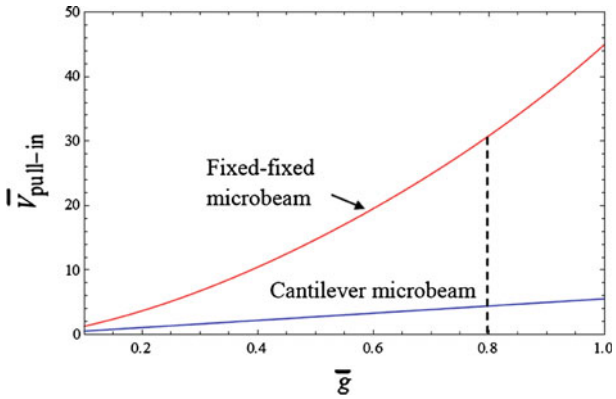

Fig. 6 Effect of normalized electrostatic gap and boundary conditions on normalized pull-in voltage of the RF-MEMS switch

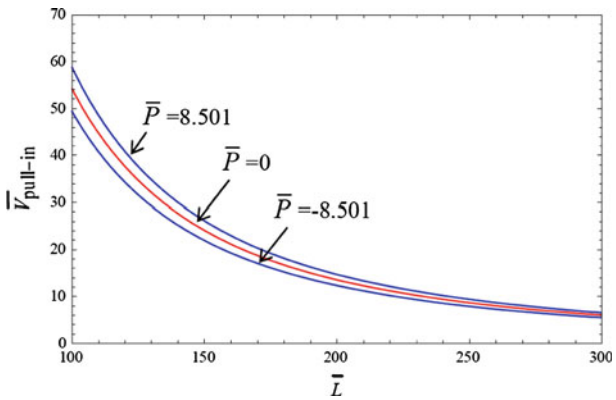

Fig. 7 Effect of microbeam geometry and initial residual load on normalized pull-in voltage of the RF-MEMS switch

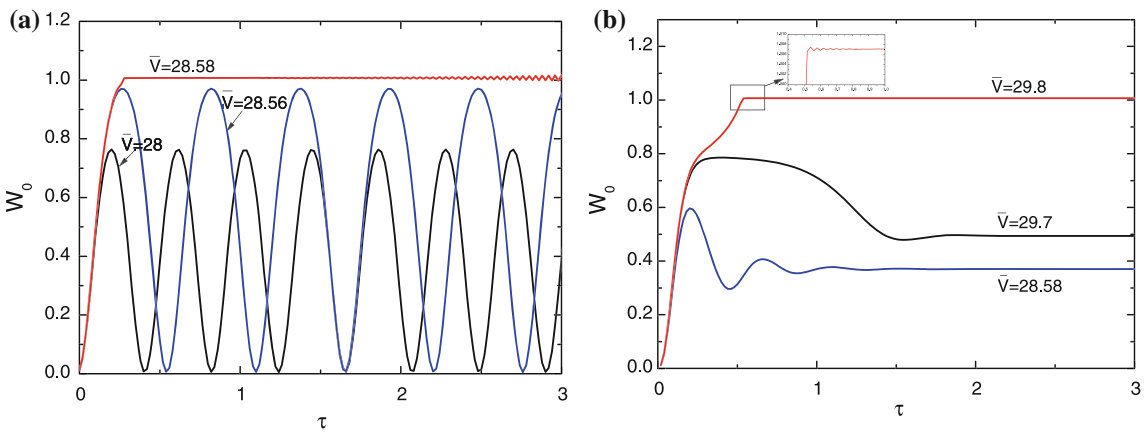

Fig. 8 Dynamic pull-in of the RF-MEMS switch. **a** without damping; **b** with damping

system. If we now consider the squeeze membrane damping with $\alpha_1 = 3$ and assuming a contact damping parameter $\beta_2 = 0.001$, the dynamic pull-in voltage increases to 29.8, which is comparable to the static pull-in voltage. This is because the kinetic energy of the system decays rapidly due to damping, and dynamic effects are thus diminished. Comparing Fig. 8a and b, it can be observed that, as expected, damping increases the normalized dynamic pull-in voltage of MEMS switches. Unlike Fig. 8a, the insert in Fig. 8b shows the dramatic damping of the oscillatory bouncing following the pull-in.

The long-term reliability of MEMS switches is a major concern for RF and microwave applications. The dynamics of the switch is related to its reliability and performance. This is because the impact force and

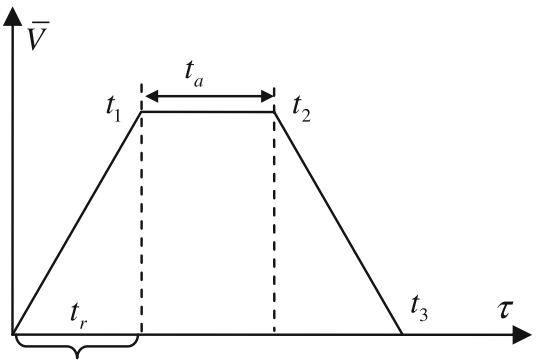

Fig. 9 Assumed waveform of input voltage

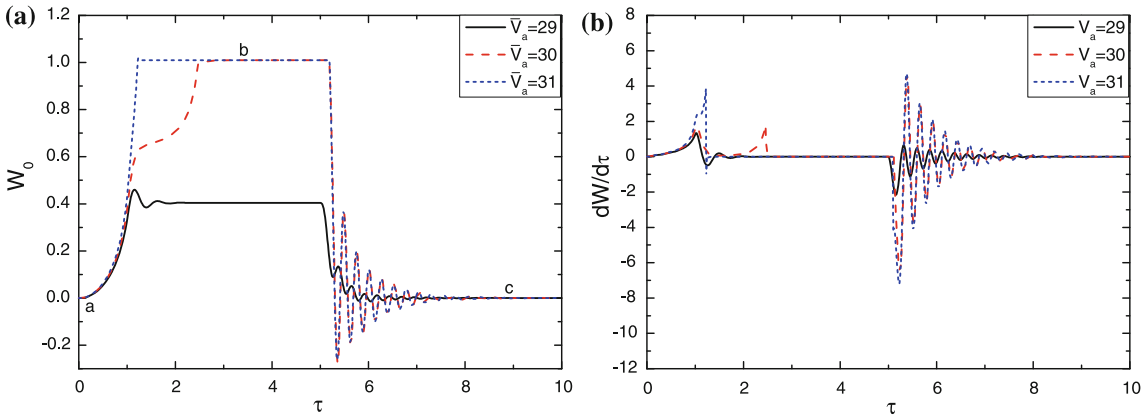

Fig. 10 Closure and opening of the RF-MEMS switch. **a** Deflection response of the midpoint of the microbeam; **b** velocity response of the midpoint of the microbeam

bounce of the switch during contact may lead to the deterioration of the contact interfaces [1,17,18,23,44]. Stiction is another challenge to the commercial deployment of RF-MEMS switches. In this case, when the actuation signal is removed, the switch fails to recover its original position due to the surface forces (such as Van der Waals force and Casimir force) between the switch and the substrate. Thus, the desired switch is characterized by minimal close time with a soft landing during closure and without stiction during opening. In this section, we assess the reliability and study the closure and opening process of the switch to examine its contact bouncing and stiction characteristics. We simulate the time history of a shunt switch subjected to the voltage shown in Fig. 9, as follows:

$$\bar{V}(\tau) = \begin{cases} \frac{\bar{V}_a}{t_r}\tau & 0 \le \tau < t_1 \\ \bar{V}_a & t_1 \le \tau < t_2 \\ -\frac{\bar{V}_a}{t_r}(\tau - t_3) & t_2 \le \tau < t_3 \\ 0 & t_3 \le \tau \end{cases} \tag{32}$$

where t_r is the rise time, t_a is the actuation time, $t_1 = t_r$, $t_2 = t_1 + t_a$, and at $t_3 = t_2 + t_r$ the voltage is removed. In this paper, the rise time is defined as the time taken by the microbeam to transition from zero to peak voltage. The fall time, which is defined as the time to ramp down from peak to zero volts, is chosen to be equal to the rise time. A rise time of 0 represents a step. The shapes of the rise and fall are discussed in [44]. Here, we use the linear ramps depicted in Fig. 9.

From Fig. 10, it can be observed that the switch begins from a flat position 'a' representing ON-state and settles down to Off-state at 'b' and returns back to the flat position after release to the open switch state at 'c'. It can be noticed that there is no contact bouncing during the closure, which demonstrates a superior performance to series switches [18,47]. Moreover, after the actuation voltage is removed, the microbeam loses contact with

the dielectric layer and experiences no stiction in spite of the presence of the Van der Waals force and Casimir force.

Let us now consider the case when the actuation voltage is less than the dynamic pull-in voltage. Figure 10a shows that the switch cannot be pulled down in the case where $\bar{V}_a = 29$ and $W_0 = 0.4$ (not unity). When the actuation voltage is larger than the dynamic pull-in voltage (e.g., the case where $\bar{V}_a = 31$), the switch closes much faster. Figure 10b shows the effect of the pull-in voltage upon the response of the microbeam. It reveals that higher actuating voltage can lead to higher impact loads as a result of the introduction of high contact speeds.

The effect of normalized damping coefficients upon the response of the microbeam is presented in Fig. 11. As expected, larger normalized damping leads to slower response in terms of the microbeam's deflection and velocity. It is worth noting that the overdamped case leads to excessive closure time. The undamped case will lead to excessive bouncing, as seen in Fig. 11.

Figure 12 depicts the response of the microbeam with different rise and actuating times. It can be observed that when the rise and the fall times are relatively long, the vibration amplitude of the microbeam is reduced and there is less capacitive vibration when the actuating voltage is removed. On the other side, it takes relatively longer time to close the switch.

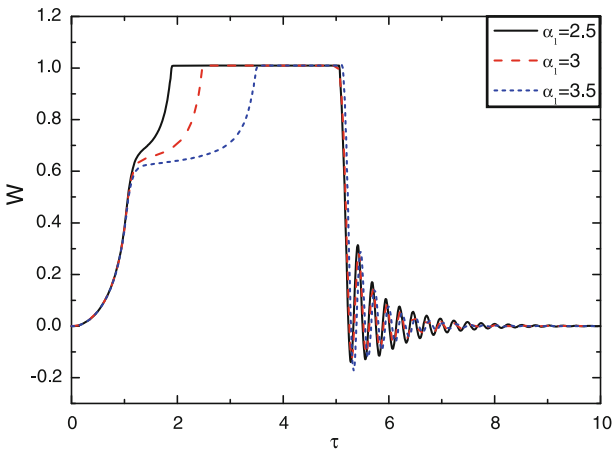

Fig. 11 Effect of damping on the dynamic response of the midpoint of the microbeam ($t_r = 1$, $t_a = 4$, and $\beta_2 = 0.01$)

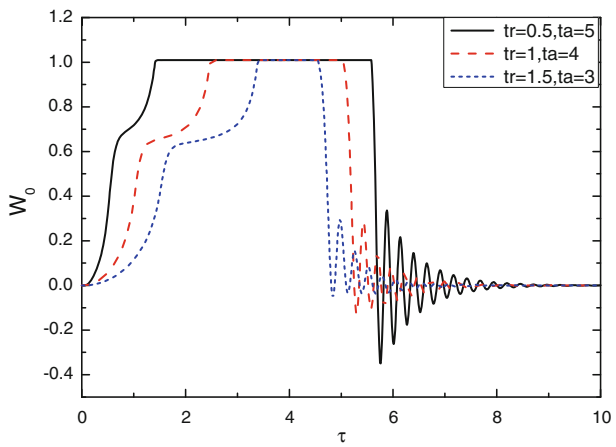

Fig. 12 Effect of different rise and fall times on the dynamic response of the midpoint of the microbeam ($\alpha_1 = 3$ and $\beta_2 = 0.01$)

4 Conclusions

In this paper, a unified and comprehensive analytical model is developed to simulate the complete static and dynamic responses of microactuators during free flight, impact and contact with the dielectric layer. The model incorporates the couple stress theory to introduce an intrinsic length scale as a state variable and examines its effect on the response RF-MEMS switches. The model further considers nonlinear contact force, Van der Waals force, Casimir force and squeeze-film damping effects upon the actuating voltage pull-in and the response of the microbeam switch. Two support types (Cantilever and fixed–fixed supports) are examined, and the effects of the presence of initial residual loading, electrostatic gap and the geometry of the microbeam on the pull-in and post pull-in voltages are evaluated and discussed. The work was further extended to account for inertial stiffening and dynamic bouncing. Our findings reveal that the developed model can be adapted for the design of RF-MEMS switches.

Acknowledgments The funding provided by the Chinese Scholarship Council (CSC), Qatar National Research Fund NPRP 09-508-2-192 and the Natural Sciences and Engineering Research Council of Canada (NSERC) is gratefully acknowledged. We thank the reviewers of this article for their helpful and insightful suggestions.

References

1. Gabriel, M., Rebeiz, R.F.: RF MEMS Theory, design and technology. Wiley, Hoboken (2003)
2. Yao, J.J.: RF MEMS from a device perspective. J. Micromech. Microeng. **10**, R9 (2000)
3. Rebeiz, G.M., Muldavin, J.B.: RF MEMS switches and switch circuits. IEEE Microw. Mag. **2**, 59 (2001)
4. Schiele, I., Hillerich, B., Kozlowski, F., Evers, C.: Micromechanical relay with electrostatic actuation. In: IEEE, vol. 2, p. 1165 (1997)
5. Gupta, R.K., Hung, E.S., Yang, Y.J., Ananthasuresh, G.K., Senturia, S.D.: Pull-in dynamics of electrostatically-actuated beams. Technical Digest Solid State Sensor and Actuator Workshop. Hilton Head Island, SC, p. 3 (1996)
6. Nielson, G.N., Barbastathis, G.: Dynamic pull-in of parallel-plate and torsional electrostatic MEMS actuators. J. Microelectromech. Syst. **15**, 811 (2006)
7. Nayfeh, A.H., Younis, M.I., Abdel-Rahman, E.M.: Dynamic pull-in phenomenon in MEMS resonators. Nonlinear Dyn. **48**, 153 (2007)
8. Fargas-Marques, A., Shkel, A.M.: On electrostatic actuation beyond snapping condition. IEEE, p. 4 (2005)
9. Fargas-Marques, A., Costa Castello, R., Shkel, A.M.: Modelling the electrostatic actuation of MEMS: state of the art 2005. Available at: http://bibliotecnica.upc.es/reports/ioc/IOC-DT-P-2005-18.pdf (2005)
10. Elata, D., Bamberger, H.: On the dynamic pull-in of electrostatic actuators with multiple degrees of freedom and multiple voltage sources. J. Microelectromech. Syst. **15**, 131 (2006)
11. Carley, L.R., Bain, J.A., Fedder, G.K., Greve, D.W., Guillou, D.F., Lu, M.S.C., Mukherjee, T., Santhanam, S., Abelmann, L., Min, S.: Single-chip computers with microelectromechanical systems-based magnetic memory. J. Appl. Phys. **87**, 6680 (2000)
12. Tan, K.K., Lee, T.H., Zhou, H.X.: Micro-positioning of linear-piezoelectric motors based on a learning nonlinear PID controller. IEEE/ASME Trans. Mechatron. **6**, 428 (2001)
13. Lu, M.S.C.: Parallel-plate micro servo for probe-based data storage. Carnegie Mellon University, Pittsburgh (2002)
14. Lee, Y.K., Deval, J., Tabeling, P., Ho, C.M.: Chaotic mixing in electrokinetically and pressure driven micro flows. IEEE, p. 483 (2001)
15. Burnham, N.A., Kulik, A.J., Gremaud, G., Briggs, G.A.D.: Nanosubharmonics: the dynamics of small nonlinear contacts. Phys. Rev. Lett. **74**, 5092 (1995)
16. Steeneken, P.G., Rijks, T.G.S.M., Beek, J.T.M., Ulenaers, M.J.E., Coster, J.D., Puers, R.: Dynamics and squeeze film gas damping of a capacitive RF MEMS switch. J. Micromech. Microeng. **15**, 176 (2005)
17. Massad, J.E., Sumali, H., Epp, D.S., Dyck, C.W.: Modeling, simulation, and testing of the mechanical dynamics of an RF MEMS switch. IEEE, p. 237 (2005)
18. McCarthy, B., Adams, G.G., McGruer, N.E., Potter, D.: A dynamic model, including contact bounce, of an electrostatically actuated microswitch. J. Microelectromech. Syst. **11**, 276 (2002)
19. Rieder, W.F., Neuhaus, A.R.: Contact welding influenced by anode arc and cathode arc, respectively. IEEE, p. 378 (2004)
20. Decuzzi, P., Demelio, G.P., Pascazio, G., Zaza, V.: Bouncing dynamics of resistive microswitches with an adhesive tip. J. Appl. Phys. **100**, 024313 (2006)
21. Granaldi, A., Decuzzi, P.: The dynamic response of resistive microswitches: switching time and bouncing. J. Micromech. Microeng. **16**, 1108 (2006)
22. Gee, G., Jensen, B.D.: A Dynamic Model of Microscale Contact Breaking in RF MEMS Switches. ASME (2006)
23. Czaplewski, D.A., Dyck, C.W., Sumali, H., Massad, J.E., Kuppers, J.D., Reines, I., Cowan, W.D., Tigges, C.P.: A soft-landing waveform for actuation of a single-pole single-throw ohmic RF MEMS switch. J. Microelectromech. Syst. **15**, 1586 (2006)
24. Savkar, A.A., Murphy, K.D.: The evolution of stiction repair for microelectromechanical system cantilevers using periodic excitation. J. Sound Vib. **329**, 189 (2010)
25. Savkar, A., Murphy, K.D.: Mechanics of the dynamic release process for stiction failed micro cantilever beams using structural vibrations. Society of Photo-Optical Instrumentation Engineers, p. 68840A. 1 (2008)

26. Savkar, A.A., Murphy, K.D., Leseman, Z.C., Mackin, T.J., Begley, M.R.: On the use of structural vibrations to release stiction failed MEMS. J. Microelectromech. Syst. **16**, 163 (2007)
27. Gorthi, S., Mohanty, A., Chatterjee, A.: Cantilever beam electrostatic MEMS actuators beyond pull-in. J. Micromech. Microeng. **16**, 1800 (2006)
28. Bienstman, J., Vandewalle, J., Puers, R.: The autonomous impact resonator: a new operating principle for a silicon resonant strain gauge. Sens. Actuators A Phys. **66**, 40 (1998)
29. Liu, S., Davidson, A., Lin, Q.: Simulating nonlinear dynamics and chaos in a MEMS cantilever using Poincaré mapping. IEEE, vol. 2, p. 1092 (2003)
30. Lu, P., Zhang, P.Q., Lee, H.P., Wang, C.M., Reddy, J.N.: Non-local elastic plate theories. Proc. R. Soc. A Math. Phys. Eng. Sci. **463**, 3225 (2007)
31. Maranganti, R., Sharma, P.: Length scales at which classical elasticity breaks down for various materials. Phys. Rev. Lett. **98**, 195504 (2007)
32. Haque, M.A., Saif, M.T.A.: Strain gradient effect in nanoscale thin films. Acta Materialia **51**, 3053 (2003)
33. Maranganti, R., Sharma, P.: A novel atomistic approach to determine strain-gradient elasticity constants: Tabulation and comparison for various metals, semiconductors, silica, polymers and the (ir) relevance for nanotechnologies. J. Mech. Phys. Solids **55**, 1823 (2007)
34. Challamel, N., Wang, C.M.: The small length scale effect for a non-local cantilever beam: a paradox solved. Nanotechnology **19**, 345703 (2008)
35. Yang, F., Chong, A.C.M., Lam, D.C.C., Tong, P.: Couple stress based strain gradient theory for elasticity. Int. J. Solids Struct. **39**, 2731 (2002)
36. Park, S.K., Gao, X.L.: Bernoulli-Euler beam model based on a modified couple stress theory. J. Micromech. Microeng. **16**, 2355 (2006)
37. Ma, H.M., Gao, X.L., Reddy, J.N.: A microstructure-dependent Timoshenko beam model based on a modified couple stress theory. J. Mech. Phys. Solids **56**, 3379 (2008)
38. Fu, Y., Zhang, J.: Size-dependent pull-in phenomena in electrically actuated nanobeams incorporating surface energies. Appl. Math. Model. **35**, 941 (2011)
39. Sun, L., Han, R.P.S., Wang, J., Lim, C.T.: Modeling the size-dependent elastic properties of polymeric nanofibers. Nanotechnology **19**, 455706 (2008)
40. Li, X.F., Wang, B.L., Lee, K.Y.: Size effects of the bending stiffness of nanowires. J. Appl. Phys. **105**, 074306 (2009)
41. Fu, Y., Zhang, J.: Electromechanical dynamic buckling phenomenon in symmetric electric fields actuated microbeams considering material damping. Acta Mech. **215**, 29 (2010)
42. Xu, L., Jia, X.: Electromechanical-fluidic coupled dynamics for microbeams. Proc. Inst. Mech. Eng. Part C J. Mech. Eng. Sci. **222**, 535 (2008)
43. Vyasarayani, C., Abdel-Rahman, E., McPhee, J., Birkett, S.: Modeling MEMS resonators past pull-in. J. Comput. Nonlinear Dyn. doi:10.1115/1.4002835 (2011)
44. Sumali, H., Massad, J.E., Czaplewski, D.A., Dyck, C.W.: Waveform design for pulse-and-hold electrostatic actuation in MEMS. Sens. Actuators A Phys. **134**, 213 (2007)
45. Murgude, N.C., Reddy, J.N.: Nonlinear analysis of microbeam under electrostatic loading. Mech. Adv. Mater. Struct. **13**, 13 (2006)
46. Fu, Y., Zhang, J.: Active control of the nonlinear static and dynamic responses for piezoelectric viscoelastic microplates. Smart Mater. Struct. **18**, 095037 (2009)
47. Blecke, J.C., Epp, D.S., Sumali, H., Parker, G.G.: A simple learning control to eliminate RF-MEMS switch bounce. J. Microelectromech. Syst. **18**, 458 (2009)